RNA Polymerase Alters the Mobility of an A-Residue Crucial to Polymerase-Induced Melting of Promoter DNA†

Laura Tsujikawa,‡ Michael G. Strainic,‡ Heather Watrob,§ Mary D. Barkley,*,§ and Pieter L. deHaseth*,‡

Departments of Biochemistry and Chemistry, Case Western Reserve University, 10900 Euclid Avenue, Cleveland, Ohio 44106

Received July 30, 2002; Revised Manuscript Received October 16, 2002

ABSTRACT: Strand separation in promoter DNA induced by *Escherichia coli* RNA polymerase is likely initiated at a conserved A residue at position −11 of the nontemplate strand. Here we describe the use of fluorescence techniques to study the interaction of RNA polymerase with the −11 base. Forked DNA templates were employed, containing the fluorescent base, 2-aminopurine (2AP), substituted at the −11 position in a single-stranded tail comprising the nucleotides on the nontemplate strand at which base pairing is disrupted in an RNA polymerase-promoter complex. We demonstrate that the presence of 2AP instead of an A at position −11 has no major effect on the accessibility of DNA to DNase I or $KMnO_4$ in the presence or absence of RNA polymerase, thus justifying the use of templates containing the 2AP substitution in the fluorescence studies. A blue shift of the 2AP fluorescence emission maximum is observed in the presence of RNA polymerase. The results of fluorescence anisotropy decay studies indicate that about 60% of the 2AP residues at −11 are immobilized in an RNA polymerase complex. This value is in good agreement with the fraction of 2AP-substituted templates determined to be in a stable, heparin-resistant complex with RNA polymerase. These results are consistent with the residue at −11 being tightly bound in a hydrophobic pocket of the enzyme.

In a functional or open complex between RNA polymerase[1] and a promoter, the region surrounding the start site of transcription (from −11 through +3) is single stranded (*1*−*6*). Kinetically, several intermediates have been detected on the pathway to formation of the open complex (*3*, *5*, *7*−*9*) as shown below (Scheme 1):

$$R + P \rightleftharpoons I_0 \rightleftharpoons I_1 \rightleftharpoons I_2 \rightleftharpoons RP_0$$

R is RNAP, P is the promoter, and I_0, I_1, and I_2 are intermediates. I_0 is a closed complex with no strand separation. Initiation ("nucleation") of DNA melting would occur at I_2 (*10*). I_0 and I_1, but not I_2 and RP_0, are sensitive to a challenge with heparin, a polyanionic competitor with DNA for binding to RNAP (*10*, *11*). It is thought that on promoter DNA, the melting process nucleates at the −11 position (an A in the consensus promoter sequence) (*12*−*14*), then propagates in downstream direction. An attractive hypothesis is that the initiation of the process involves "flipping" of the −11 A out of the helix (*14*−*16*). If this were the case, it would be expected that the environment of the −11 A would change dramatically upon interaction of RNAP with promoter DNA.

Gralla and co-workers (*15*, *17*, *18*) have pioneered the use of "forked DNA" templates (see Figure 1) to model aspects of an RNAP−promoter complex in which the nucleation of DNA melting had occurred (I_2 or RP_0 in Scheme 1). These templates emulate the boundary between double-stranded and single-stranded DNA: the region from position −40, including the −35 element, through the first base pair of the −10 element (at position −12), is double helical but the 3′ end of the nontemplate strand, including just the −11 A ("Short Fork") of the consensus −10 sequence, or additional nucleotides ("Long Fork"), is unpaired. Forked templates have been the recent focus of structural studies (*19*). Just as is the case with promoter DNA, several kinetic intermediates have been detected on the pathway to formation of a final, heparin-resistant complex between RNAP and forked DNA (*20*) (Scheme 2):

$$R + F \rightleftharpoons RF_1 \rightleftharpoons RF_2 \rightleftharpoons RF_3$$

R again represents RNAP, F is the forked DNA, RF_1 is a heparin-sensitive intermediate, and RF_2 and RF_3 are heparin-resistant complexes. These results indicate that, with the forked template, DNA downstream of −11 is not necessary for triggering progression through the intermediates RF_1 and RF_2 (*20*) and that at equilibrium heparin-resistant and heparin-sensitive complexes coexist in solution. The distribution between these complexes is sensitive to forked DNA sequence.

Detection of an interaction between RNAP and the −11 A upon formation of an RNAP−DNA complex would advance our understanding of the mechanism of RNAP induced DNA melting: evidence for tight binding of the −11

† This work was supported by NIH Grants GM31808 (PLD) and GM52263 (MDB).

* To whom correspondence should be addressed. E-mails: mdb4@po.cwru.edu, pld2@po.cwru.edu.

‡ Department of Biochemistry.

§ Department of Chemistry.

[1] Abbreviations: 2AP, 2-aminopurine; DCM, 4-dicyanomethylene-2-methyl-6-(*p*-dimethylaminostryl)-4H-pyran; DEPC, diethyl pyrocarbonate; DTT, dithiothreitol; EDTA, ethylenediaminetetraacetic acid; EMSA, electrophoretic mobility shift assay; HEPES, *N*-2-hydroxyethylpiperazine-*N*′-2-ethanesulfonic acid; RNAP, *E. coli* RNA polymerase; Tris, tris-(hydroxymethyl)-aminomethane.

10.1021/bi026539m CCC: $22.00
Published on Web 11/26/2002

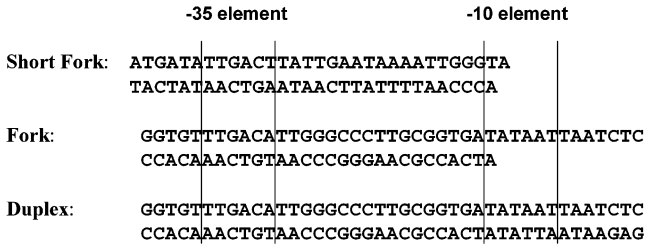

FIGURE 1: The DNA templates employed in this study. The sequence of the Short Fork template is based on that of the P_R' promoter of bacteriophage lambda. Vertical lines denote the −35 and (partial) −10 sequences. This template has a one base single-stranded overhang (the −11 A). The numbering scheme employed in this paper is consistent with the −10 sequence TATAAT extending from −12 to −7, as it does in most promoters (i.e., the right-most base pair of the Duplex DNA would be the start site of RNA synthesis). The bottom two templates are loosely based on the sequence of the P_{RM} promoter of bacteriophage λ. Their nontemplate strand extends an additional 11 bases in the downstream direction. This stretch and the −11 A are single stranded for the Fork and double stranded for the Duplex templates. Also used in this work are 2AP Fork and 2AP Duplex, which are similar to wt Fork and wt Duplex, respectively, but each bear a 2AP substitution for the −11 A.

A to RNAP would be consistent with, although not in and of itself constitute proof of, a base flipping mechanism for the nucleation of DNA melting. We have addressed this issue by using forked DNA to deliver the fluorescent base 2AP, substituted for the A at position −11, in the proper position for any interaction with RNAP to occur. 2AP is an analogue of adenine that can form two stable hydrogen bonds with thymine in the Watson−Crick geometry (*21*). It has been widely used as a fluorescent probe for the environment of A's at particular positions in DNA. Any tight interaction with RNAP would then be revealed by fluorescence techniques. The results obtained indicate that (1) the fraction of RNAP−DNA complexes for which the DNA is bound sufficiently tightly to resist a challenge with heparin is not greatly reduced due to the substitution of A by 2AP at −11, (2) at the resolution of footprinting and chemical probing techniques, complexes between RNAP and forked DNA are not affected by the presence of a 2AP at −11, and (3) the mobility of this 2AP is greatly reduced upon formation of a stable RNAP−forked DNA complex, consistent with its tight binding in a pocket on the RNAP.

EXPERIMENTAL PROCEDURES

Materials. Oligonucleotides were synthesized by Gibco BRL or Genset. If necessary, they were purified by electrophoresis on 15% denaturing gels; the appropriate band was excised, and the DNA was eluted by diffusion and finally recovered by passage through C18 columns. Extinction coefficients of forked templates at 260 nm, ϵ(260), were estimated using 1 A(260) unit = 50 μg/mL for double-stranded DNA and 1 A(260) unit = 33 μg/mL for single-stranded DNA and summing the values for single- and double-stranded regions of the DNA. 2AP riboside was a generous gift from Dr. Lawrence C. Sowers (Loma Linda University School of Medicine). [γ-^{33}P]ATP, [γ-^{32}P]ATP, and [α-^{32}P] UTP were from New England Nuclear. DNA modifying enzymes were purchased from either New England Biolabs or Roche Molecular Biochemicals. *E. coli* RNAP core enzyme was purchased from Epicenter. RNAP holoenzyme was purified by established methods (*22*, *23*). The preparation used for the experiments shown in Figures 2−4 had a concentration of 3.2 μM and promoter DNA binding activity of (50 ± 10)%. The more concentrated preparation used for fluorescence experiments had a concentration of 16 μM and binding activity of (40 ± 10)%.

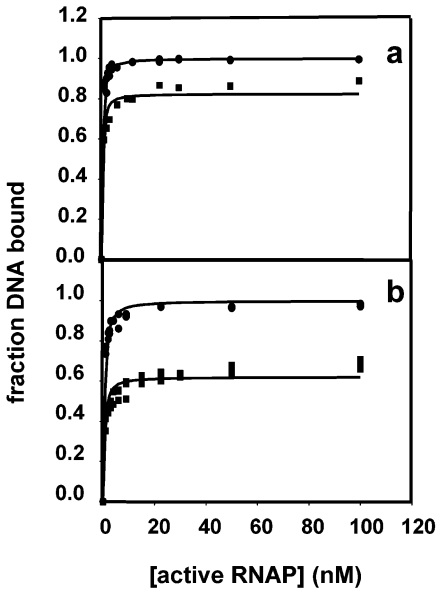

FIGURE 2: Determination of equilibrium affinities by titration of wt Fork and 2AP Fork with RNAP. The reactions contained 1 nM wt Fork and different concentrations of RNAP. Reaction mixes were analyzed by EMSA immediately (circles) or after a challenge with 100 μg/mL heparin for 10 min (squares). All data points for three separate trials are shown for 2AP Fork subjected to a heparin challenge, average values for the others. The curves shown reflect the simultaneous fits to the data points in each panel, as described in ref. *20*. (a) wt Fork (with A at −11). The best fit values are $K_1 = (1.1 \pm 0.1) \times 10^9$ M^{-1} and $K_f = 4.7 \pm 0.4$. (b) 2AP Fork (with 2AP at −11). The best fit values are $K_1 = (1.3 \pm 0.1) \times 10^9$ M^{-1} and $K_f = 1.6 \pm 0.1$.

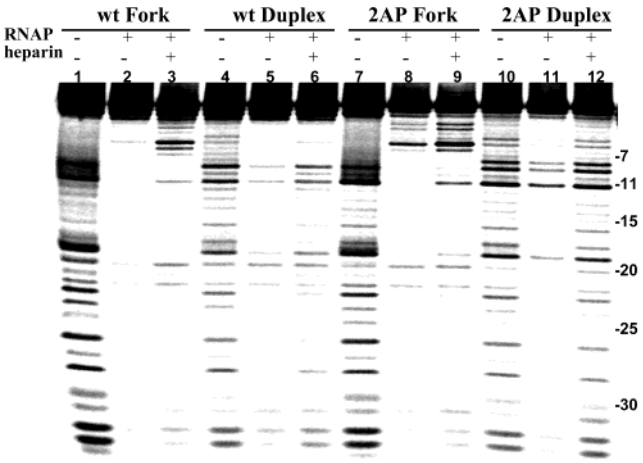

FIGURE 3: DNase I footprinting of complexes of RNAP and wt Fork or 2AP Fork. All reactions contained DNA (10 nM) labeled at the 5′ end of the nontemplate strand; RNAP (50 nM) and heparin (100 μg/mL) were added as indicated. The numbering shown to the right of the gel is based on the migration of markers generated in DEPC ("A" ladder), $KMnO_4$ ("T" ladder), and DMS ("G" ladder) modification reactions (not shown). The −10 region extends from −7 through −12. For consistency with the data shown in Figure 4, the alignment is such that the number refers to the last base removed from the 3′ end to generate the species migrating with the particular mobility.

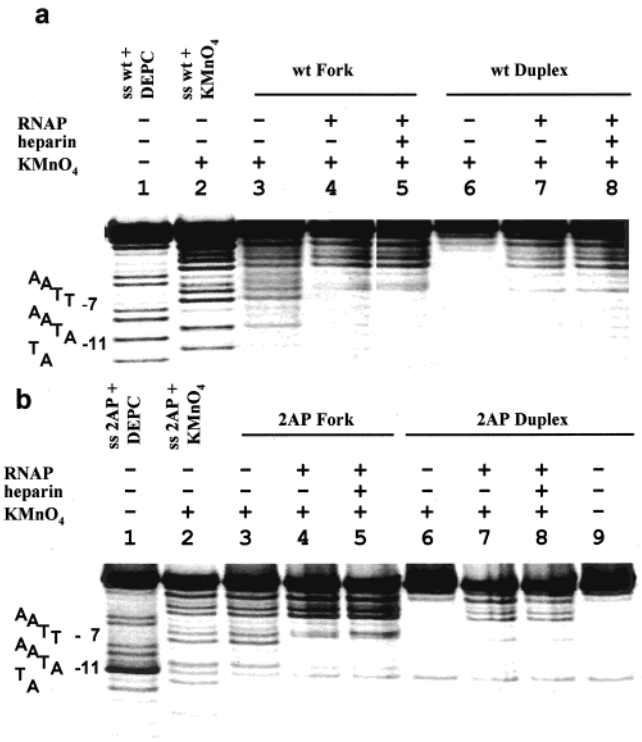

FIGURE 4: The accessibility to $KMnO_4$ of T residues of the nontemplate strand. Duplex and Fork templates, containing either −11 A or −11 2AP were probed. All reactions contained DNA (10 nM) labeled at the 5′ end of the nontemplate strand; RNAP (50 nM) and heparin (100 μg/mL) were added as indicated. The sequence shown next to the lanes was based on the bands produced by exposure of the nontemplate strand to DEPC ("A" ladder, lane 1) and $KMnO_4$ ("T" ladder, lane 2). Additions of RNAP, heparin, and $KMnO_4$ were made as indicated above the gel. (a) −11 A. (b) −11 2AP; all lanes show a faint band at −11 because some chain scission occurs at the position of 2AP just due to the addition of piperidine.

RNAP concentrations throughout the paper refer to the active enzyme.

Deoxyoligonucleotide Labeling and Annealing. 5′ end-labeling of DNA oligonucleotides was accomplished by incubation with γ-^{33}P- or ^{32}P-ATP and T4 polynucleotide kinase (New England Biolabs) using established procedures. Annealing of (partially) complementary DNA strands was as described (*20*).

Electrophoretic Mobility Shift Assay. Binding reactions were carried out as described (*20*) in reactions containing HEPES buffer (30 mM HEPES, pH 7.5, 100 mM KCl, 1 mM DTT) by titrating 1 nM of 5′ ^{32}P-labeled forked DNA at 25 °C with RNAP.[2] The samples were or were not subjected to a 10 min heparin challenge prior to loading onto a 5% nondenaturing gel, run at room temperature. Dried gels were autoradiographed and quantified by phosphorimagery (Molecular Dynamics) to determine the fraction of total radioactivity in bands corresponding to free and RNAP-bound DNA.

Data analysis was carried out using a reaction scheme, involving one intermediate (RF_1) and a final heparin-resistant complex RF_{CR} (where $[RF_{CR}] = [RF_2] + [RF_3]$) (Scheme 3):

$$R + F \overset{K_1}{\rightleftharpoons} RF_1 \overset{K_f}{\rightleftharpoons} RF_{CR}$$

For the mechanism of Scheme 3, the following two equilibrium constants can be defined:

$$K_1 = [RF_1]/([R][F]) \quad (1)$$

$$K_f = [RF_{CR}]/[RF_1] \quad (2)$$

The data collected in the presence and absence of heparin could be fit as previously described (*20*) to allow calculation of values for K_1 and K_f. The apparent binding affinity K_{app} is given by $K_{app} = K_1(1 + K_f)$. Values for the equilibrium constant K_f were found to correlate well with the relative ability of RNAP complexes to form open complexes at promoters.

DNA Footprinting and Chemical Probing. DNase I footprinting (*16*, *24*) and DEPC (*4*) and $KMnO_4$ probing (*25*, *26*) were carried out following established procedures. In all cases the DNA (10 nM, labeled at the 5′ end of one of the strands) and RNAP (50 nM) were incubated for 30 min at 37 °C prior to initiating DNase I cutting or DEPC or $KMnO_4$ modification reactions. Tests for heparin resistance involved additional incubation for 2 min in the presence of heparin (100 μg/mL). The DNase I reactions were carried out in HEPES buffer containing 10 mM $MgCl_2$. The labeled DNA was exposed to 0.025 units DNase I for 45 s at 37 °C. Reactions were terminated by adding one-fifth volume of stop solution (final concentrations: 0.375 M sodium acetate, 0.25 M β mercaptoethanol, 1 mg/mL glycogen, 62.5 μg/mL tRNA), following which the DNA was ethanol precipitated, redissolved, and analyzed on sequencing gels. To probe A residues in single-stranded regions, DEPC was added to 30%, incubation was carried out in HEPES buffer for 5 min, the reaction was terminated by addition of stop solution to the same final concentrations as shown above, and the DNA was ethanol precipitated. To probe T residues in single-stranded regions, $KMnO_4$ was added to 7.5 mM, the reaction was carried out for 3 min in HEPES buffer, stop solution (same as for DEPC) was added, and the DNA was ethanol precipitated. Following the ethanol precipitation, the DEPC and $KMnO_4$ treated DNAs were dissolved in 10% piperidine and heated to 90 °C for 20 min. The reactions were then chilled on ice and piperidine was removed either by repeated cycles of water addition and evaporation, or by ethanol precipitation in the presence of 0.5 M LiCl (*4*). Analysis was by electrophoresis on a sequencing gel.

Spectroscopic Measurements. Absorption and fluorescence measurements were made at 23 °C in 45 μL cells with 3 mm path length. The final composition of the buffer (after addition of RNAP in storage buffer to the reaction in HEPES buffer) was 30 mM HEPES, 4.5 mM Tris, pH 7.5, 0.1 M KCl, 45 mM NaCl, 10 mM $MgCl_2$, 1 mM DTT, 45 μM EDTA, and 22.5% glycerol. Samples of forked DNA alone contained 1 or 10 μM 2AP Fork. Mixtures of RNAP and forked DNA contained 2 μM 2AP Fork and 2.7 μM RNAP. Under these conditions no free 2AP Fork was detectable by EMSA. 2AP Fork concentration was determined from A(260) values measured on a Cary 3E UV−vis spectrophotometer,

[2] Data in ref *20* were analyzed using total, rather than active, RNAP concentration. This underestimates K_1 by approximately a factor of 2, but has no effect on K_f.

using the extinction coefficient $\epsilon(260) = 4.49 \times 10^5$ M^{-1} cm^{-1}. The $\epsilon(320) = 4.48 \times 10^3$ M^{-1} cm^{-1} for 2AP in 2AP Fork was calculated from A(320) using the measured DNA concentration.

Steady-state fluorescence was measured in the ratio mode on a SLM 8000C photon counting spectrofluorometer as described elsewhere (*27*). An excitation wavelength of 320 nm was used to avoid exciting the tryptophans in RNAP. Fluorescence quantum yields Φ were determined relative to quinine sulfate in 1 N H_2SO_4 using a value of 0.549 at 23 °C (*28*). To reduce errors due to low absorbance of 2 μM 2AP Fork at 320 nm, 2AP absorbance of these solutions was calculated from the absorbance measured at 260 nm times the $\epsilon(320)/\epsilon(260)$ ratio. The $\epsilon(320)$ of 2AP Fork was assumed to be the same in the absence and presence of RNAP.

Fluorescence decays were measured by time-correlated single photon counting using a picosecond DCM dye laser system as described elsewhere *(27*, 29). Decay curves were acquired at 370 nm emission wavelength (16-nm band pass) in 1024 channels of 13−52 ps/channel using a PCA3 multichannel analyzer (Oxford Instruments). Counts in the peak channel were $>1-5 \times 10^3$ for samples with 1 or 2 μM 2AP Fork and $\geq 5-20 \times 10^3$ with 10 μM 2AP Fork. Decay data were deconvolved in the Beechem global program (*30*). Goodness of fit was judged by reduced chi square χ_r^2 and autocorrelation function of the weighted residuals.

Fluorescence intensity decays $I(t)$ were fit to a sum of exponentials

$$I(t) = \sum \alpha_i \exp(-t/\tau_i) \quad (3)$$

with amplitudes α_i and lifetimes τ_i. The amplitude-weighted lifetime $\bar{\tau} = \Sigma\alpha_i\tau_i/\Sigma\alpha_i$. Data sets acquired under different experimental conditions (concentration, number of peak counts, and time scale) were analyzed simultaneously with lifetimes but not amplitudes constrained to be the same in all the decay curves.

Conformational states and relative populations of 2AP in 2AP Fork were determined from fluorescence quantum yield and lifetime data as described by Rachofsky et al. (*31*, *32*). The fraction of intrahelical stacked 2AP f_s was calculated from

$$f_s = 1 - \Phi_{rel}/\tau_{rel} \quad (4)$$

Here $\Phi_{rel} = \Phi/\Phi_{2AP}$ and $\tau_{rel} = \bar{\tau}/\tau_{2AP}$ are the quantum yield and amplitude-weighted lifetime of 2AP in 2AP Fork relative to the free 2AP nucleoside. For 2AP riboside, $\Phi_{2AP} = 0.74 \pm 0.02$ and $\tau_{2AP} = 10.7$ ns. The quantum yield and lifetime of 2AP deoxyribo- and ribonucleoside are the same (*31*, *33*).

Fluorescence anisotropy decays $r(t)$ were fit to a sum of exponentials with preexponential β_i and rotational correlation

$$r(t) = \sum \beta_i \exp(-t/\phi_i) \quad (5)$$

time ϕ_i. The initial anisotropy $r(0) = \Sigma\ \beta_i$. Individual polarized decays $I_{VV}(t)$ and $I_{VH}(t)$ were deconvolved simultaneously with a magic angle decay $I(t)$

$$I_{VV}(t) = I(t)[1 + 2r(t)]/3 \quad (6a)$$

$$I_{VH}(t) = GI(t)[1 - r(t)]/3 \quad (6b)$$

where the correction factor $G \sim 1$ in our instrument. The global analysis constrained the lifetimes τ_i to be the same in all three decay curves, and the preexponentials β_i and rotational correlation times ϕ_i to be the same in the two polarized decays.

RESULTS

The experiments described here employ a forked template ("Fork"; see Figure 1), loosely based on the P_{RM} promoter of bacteriophage lambda, that has a double-stranded upstream region and a 12 nucleotide single-stranded DNA overhang beginning at position −11. In this respect the templates described in this paper differ from those we used previously (*16*, *20*), which had only a one base overhang, namely the A at −11 ("Short Fork", see Figure 1). The extended overhang not only allows probing of interactions with RNAP over almost the entire stretch of DNA that becomes single stranded in an open complex, but was also advantageous in providing a longer substrate for the footprinting and chemical probing experiments. To lay the foundation for fluorescence experiments utilizing DNA with a 2AP substitution at −11, we compared the behavior of several DNAs and RNAP−DNA complexes containing A and 2AP at this position. Below we present the results of our studies of the effect of 2AP on the partitioning of RNAP−forked DNA complexes into stable (heparin-resistant) and unstable (heparin-sensitive) complexes and on the structural perturbations of the DNA in these complexes. We then describe the use of 2AP fluorescence to study the interaction of RNAP with the −11 base.

Effect of −11 2AP on Partitioning into Heparin-Sensitive and -Resistant RNAP−Forked DNA Complexes. We followed the procedure outlined by Tsujikawa et al. (*20*): binding isotherms were obtained for the formation of complexes between RNAP and wt or 2AP Fork (see Figure 1), with or without a short challenge with heparin (Figure 2). Determination of the distribution of complexes by addition of heparin is justified because the time of the challenge is short compared to the half-life of the heparin-resistant complexes. Formation of a final heparin-resistant complex (RF_{CR}) with RNAP was previously shown to proceed through a heparin-sensitive intermediate (RF_1) (see ref *20* and Experimental Procedures). By simultaneous fitting of data obtained with or without a heparin challenge, values for K_1 and K_f can be obtained. The values for K_f are largely derived from the fraction of the complexes that prove to be resistant to the heparin challenge. For wt Fork, $K_1 = (1.1 \pm 0.1) \times 10^9$ M^{-1} and $K_f = 4.7 \pm 0.4$ (Figure 2a); $K_{app} = 6.3 \times 10^9$ M^{-1}. For 2AP Fork, $K_1 = (1.3 \pm 0.1) \times 10^9$ M^{-1} and $K_f = 1.6 \pm 0.1$ (Figure 2b); $K_{app} = 3.4 \times 10^9$ M^{-1}.

While the 2AP substitution apparently does not significantly affect the initial binding event (K_1 is about the same), it decreases, but does not abolish, the propensity of RNAP and 2AP Fork to form heparin-resistant complexes: K_f is reduced by a factor of 3. As a result, approximately 83% of the complexes present at equilibrium, are heparin resistant if the −11 base is A, but only 62% if the −11 base is 2AP. The 2AP substitution does not affect the stability of the heparin-resistant complex: within experimental error the half-lives for complexes containing wt and 2AP Fork are similar (about 6 h; data not shown). The fits to the "no

Table 1: Fluorescence Data[a]

parameter	DNA template	
	2AP Fork[b]	RNAP−2AP Fork complex[c]
emission peak	369 nm	364 nm
quantum yield Φ	0.032 ± 0.005	0.044 ± 0.003
	lifetime ns (amplitude)[d]	
τ_1 (α_1)	7.0 (0.08 ± 0.003)	7.4 (0.13 ± 0.05))
τ_2 (α_2)	2.3 (0.13 ± 0.01)	2.4 (0.10 ± 0.02)
τ_3 (α_3)	0.48 (0.23 ± 0.03)	0.53 (0.18 ± 0.03)
τ_4 (α_4)	0.07 (0.43 ± 0.04)	
$\bar{\tau}$	1.15	3.16
	rotational correlation time ns (preexponential)[e]	
ϕ_1 (β_1)	0.18 ± 0.07 (0.26 ±0.03)	1.40 ± 0.01 (0.13 ± 0.02)
ϕ_2 (β_2)	18 ± 4 (0.09 ± 0.03)	110 ± 40 (0.22 ± 0.01)
$r(0)$[f]	0.35 ± 0.04	0.35 ± 0.02

[a] Excitation wavelength 320 nm, emission wavelength 370 nm, 23 °C. [b] Concentrations: 1 and 10 μM. [c] Concentrations: 2 μM 2AP Fork, 2.7 mM RNAP. [d] Global analysis of 10 decay curves for 2AP Fork, global $\chi_r^2 = 1.23$. Global analysis of 12 decay curves for RNAP−2AP Fork, global $\chi_r^2 = 1.15$. Amplitudes α_i scaled to the relative steady-state intensity at 370 nm: $\sum\alpha_i\tau_i = 1.00$ for 2AP Fork; $\sum\alpha_i\tau_i = 1.30$ for RNAP−2AP Fork, stray light component omitted. [e] Mean values and standard deviations of anisotropy decay parameters from three experiments at 370 nm emission wavelength. [f] Literature values for 2AP in DNA are 0.26−0.30 at 300 nm excitation wavelength (*39*) and 0.331−0.377 at 317 nm excitation wavelength (*33*).

heparin" data in Figure 2 yield binding constants of 3.6×10^9 M^{-1} for wt Fork and 2.9×10^9 M^{-1} for 2AP Fork. Experiments performed on Short Fork DNAs (see Figure 1) with an overhang consisting of just the −11 A showed a more drastic effect of 2AP substitution for the −11 A: no heparin-resistant complex could be detected (data not shown). The observation of only modest effects of 2AP substitution when the single-stranded overhang is longer likely reflects the fact that sequences downstream of −11 greatly increase the propensity of complexes with RNAP to isomerize to a heparin-resistant form (*18*, *20*). Even in the absence of a heparin-challenge, an effect of the presence of 2AP on the interaction of Short Fork with RNAP is apparent: the measured binding constant was 1.3×10^7 M^{-1} if the base at −11 is 2AP (data not shown), 2 orders of magnitude less than the value obtained if −11 is an A (*20*).

Effect of −11 2AP on the Structure of RNAP−DNA Complexes. DNase I footprinting data for the top (nontemplate) strand of wt Fork, 2AP Fork, wt Duplex, and 2AP Duplex are shown in Figure 3. In the absence of added RNAP, the observed patterns are similar for wt and 2AP Fork, but not for wt and 2AP Duplex (Figure 1). The most striking effect of the substitution is that the A at −8 becomes more sensitive to cleavage (compare Figure 3, lanes 4 and 10); subtle changes include the G at −18 (increased sensitivity) and the Ts at −12 and −20 (decreased sensitivity). These multiple changes may reflect perturbations of DNA conformation, or an effect of 2AP on the interaction of DNase I with the Duplex. The patterns of bands obtained in the −10 region and upstream for RNAP-bound forked DNAs and wt Duplex, with or without heparin challenge, and for 2AP Duplex without heparin challenge, are very similar to each other and to those obtained for promoter DNA in complex with RNAP. The spacer DNA separating the −10 and −35 regions is almost entirely protected, except for a stretch in the middle (positions −20 to −22 of the nontemplate strand and −23 to −26 on the template strand; data not shown). This is typical of footprints seen at promoters (*34*). We conclude that for the forked DNAs, the footprint is not affected by the substitution of a 2AP at −11 and that their mode of interaction with RNAP is similar to that of promoter DNA. For heparin-challenged complexes of RNAP and Fork DNA with either −11 A or −11 2AP, hypersensitive sites become visible downstream of the −10 region for nucleotides at −2 and −1 (compare lanes 1 and 3, and 7 and 9). Little cutting is observed in this region with either the free Fork or the Duplex DNA, indicating that the RNAP-bound forked DNA must have unique accessibility to DNase I in the presence of heparin. We speculate that the heparin displaces the single-stranded DNA tail downstream of −7 from the RNAP by binding in the nontemplate groove (*19*), and that the displaced region of the single-stranded DNA then adopts a particularly DNase I sensitive conformation. For the 2AP Duplex, the pattern for the heparin-challenged complex is similar to that of the free DNA. As described below (see Figure 4b), even in the presence of heparin, the $KMnO_4$ sensitivity of 2AP Duplex is RNAP-dependent, demonstrating the existence of stable, strand-separated RNAP−2AP Duplex complexes as well. We conclude that in the presence of heparin, 2AP Duplex bound to RNAP and free 2AP Duplex coexist in solution, with the former giving rise to the banding pattern produced by $KMnO_4$, and the latter to the one resulting from DNase I cutting.

To probe in more detail the effect of 2AP on the interaction of RNAP with regions of single-stranded DNA already present in the Fork templates or generated by RNAP on the Duplex templates, complexes with RNAP were treated with $KMnO_4$, which preferentially oxidizes T residues in single-stranded regions of DNA. The data for the nontemplate strand are shown in Figure 4. The presence of 2AP at −11 enhanced the sensitivity of the DNA to piperidine (the distinct band visible at −11 in lanes 2−9 of Figure 4b is absent for untreated DNA; data not shown) and, dramatically, to DEPC (Figure 4b, lane 1). The banding patterns for wt and 2AP Fork are similar. The base pair at −12 is protected (compare lanes 2 and 3, most evident in Figure 4b), indicating a lack of significant "fraying" for this base pair at the edge of the helix, likely due to the single-stranded overhang. The patterns for the two forked DNA templates are similar in the presence of RNAP as well, demonstrating that the 2AP substitution does not significantly affect the interaction of RNAP with single-stranded regions of the Fork. In both cases protection of the −7 and −10 bases from $KMnO_4$ attack is observed. These patterns are but little affected by a heparin challenge.

The T's of the Duplex templates are well-protected in the absence of added RNAP, as expected for double-stranded DNA (compare lanes 3 and 6 of Figures 4a and 4b). Addition of RNAP leads to patterns similar to those observed for the Fork templates. While the bands are of similar intensity for complexes of wt Fork and wt Duplex (Figure 4a, compare lanes 4 and 7, and 5 and 8) they are less intense for the 2AP Duplex than for the 2AP Fork (Figure 4b, compare lanes 4 and 7, and 5 and 8), indicating that RNAP-induced melting is incomplete with a 2AP at −11. Addition of heparin reduces the intensities of the bands for the 2AP Duplex (compare lanes 7 and 8 in Figure 4b). We conclude that almost all RNAP−DNA complexes survive the heparin challenge if the DNA has a −11 A, and a smaller, but significant fraction if it has a −11 2AP. The latter was not observed in the DNase I footprinting experiments (Figure 3, lane 12), as the DNase I pattern largely reflected the free DNA in the solution. Probing of the template strand (not shown) reveals that in the presence of RNAP several Ts, including those opposite both −11 A and −11 2AP, become accessible to $KMnO_4$ modification. This again shows that at least some RNAP-induced strand separation occurs for the 2AP Duplex.

2AP Fluorescence. Fluorescence quantum yields, lifetimes, and anisotropy decays were measured at 23 °C for 2AP Fork in the presence and absence of RNAP (Table 1). At 320 nm excitation wavelength, only emission from 2AP was detected. The emission from solutions of RNAP alone was indistinguishable from buffer in both steady-state and time-resolved measurements. However, tryptophan fluorescence of RNAP was detectable at lower excitation wavelengths (<315 nm). The emission spectrum of 2AP Fork shifted 5 nm to the blue upon binding of RNAP. A 5 nm blue shift was also reported for the complex of T4 DNA polymerase with 2AP substituted primer-template DNA (*35*). The lowest absorption band of 2AP is a $\pi \rightarrow \pi^*$ transition (*36*, *37*), and the emission spectrum is blue shifted in nonpolar solvents (*36*, *38*). The 5 nm blue shift is consistent with transfer of the fluorescent base to a more hydrophobic environment in the RNAP−2AP Fork complex.

As commonly observed upon incorporation of 2AP into polynucleotides, the quantum yields and amplitude-weighted lifetimes of free and bound 2AP Fork dropped dramatically relative to 2AP riboside, and the fluorescence decay went from monoexponential to multiexponential. Global analysis of 10 or 12 decay curves for each sample gave reasonable fits to three exponential functions. However, four exponential functions improved the χ_r^2 values. In 2AP Fork, the lifetime of the fourth component is 70 ps. Three or four exponential decays with lifetimes from 0.03 to 10 ns have been reported for 2AP in DNA (*32*, *33*, *39*). In RNAP−2AP Fork complex, the lifetime of the fourth component was shorter (1−10 ps) and is probably due to light scattering by RNAP (<2% of total intensity). Five exponential fits gave no improvement in χ_r^2. Table 1 shows the results of the four exponential fits omitting the stray light component for the RNAP complex. The amplitude-weighted lifetime of 2AP Fork increased almost 3-fold in the presence of RNAP.

In contrast, the quantum yield increased only about 40% in bound compared to free 2AP Fork. Combining fluorescence quantum yield and lifetime data can identify local conformational states of 2AP in DNA (*31*, *32*). Model studies show that the fluorescence quenching is due to two types of

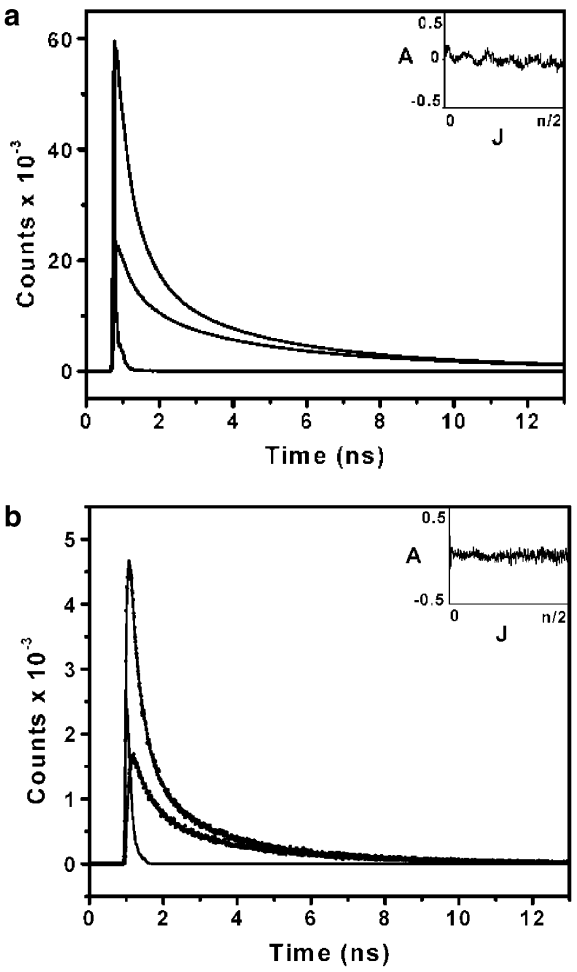

FIGURE 5: Fluorescence anisotropy decay data for 2AP Fork and RNAP−2AP Fork complex. The left curve is the instrumental response, points are $I_{VV}(t)$ (higher) and $I_{VH}(t)$ (lower), and smooth curves through points are best fits from global analysis. The autocorrelation function of the weighted residuals (inset) is shown for $I_{VV}(t)$. (a) Decay parameters for 2AP Fork: $\tau_1 = 7.2$ ns ($\alpha_1 = 0.07$), $\tau_2 = 2.5$ ns ($\alpha_2 = 0.12$), $\tau_3 = 0.59$ ns ($\alpha_3 = 0.31$), $\tau_4 = 0.11$ ns ($\alpha_4 = 0.26$) with $\Sigma\, \alpha_i\, \tau_i = 1.00$; $\phi_1 = 0.15$ ns ($\beta_1 = 0.26$), $\phi_2 = 20$ ns ($\beta_2 = 0.13$); global $\chi_r^2 = 1.87$. (b) Decay parameters for RNAP−2AP Fork complex: $\tau_1 = 6.8$ ns ($\alpha_1 = 0.10$), $\tau_2 = 1.9$ ns ($\alpha_2 = 0.25$), $\tau_3 = 0.40$ ns ($\alpha_3 = 0.34$) with $\Sigma\, \alpha_i\, \tau_i = 1.30$, stray light component omitted; $\phi_1 = 1.4$ ns ($\beta_1 = 0.11$), $\phi_2 = 90$ ns ($\beta_2 = 0.23$); global $\chi_r^2 = 1.46$.

interactions: aromatic base stacking and collisions with neighboring bases (*31*). Base stacking in the appropriate geometry quenches by a static mechanism due to formation of a nonfluorescent ground-state complex (*31*). It reduces the quantum yield, but not the lifetime. Collisions with other bases quench by a dynamic mechanism, which lowers quantum yield and lifetime proportionally. The efficiencies of static and dynamic quenching are the same for all the natural bases. The fraction of stacked 2AP, f_s, was calculated from quantum yield and lifetime data for 2AP Fork using eq 4. The values of f_s are 0.62 ± 0.07 in the absence of RNAP and 0.80 ± 0.02 in the presence of RNAP. The longest lifetime for 2AP in free or bound 2AP Fork is ∼7 ns, which is lower than the 10.7 ns lifetime of 2AP riboside. This suggests that 2AP does not adopt a completely unquenched, extrahelical conformation (*32*). The fraction of unstacked 2AP, $f_u = 1 - f_s$ comprises fluorescent species with lifetimes from 0.07 to 7.0 ns in the absence of RNAP

and 0.53 to 7.4 ns in the presence of RNAP, presumably representing partially unstacked conformations of 2AP. On the basis of the amplitudes α_i, the longest lifetime component accounts for the increase in quantum yield of the RNAP complex compared to DNA alone.

The anisotropy decay data of both free and bound 2AP Fork were best fit by two exponential functions. Figure 5a shows an experiment for 2AP Fork with about 20×10^3 peak counts. Similar results were obtained from an experiment with only about 5×10^3 peak counts. The subnanosecond rotational correlation time of 2AP Fork is typical of literature values for short DNA duplexes and represents rapid internal motion of the base in DNA (*39*). The 18 ns correlation time represents overall tumbling of the DNA. Five rotational correlation times ranging from 14 to 83 ns were calculated for a molecular model of 2AP Fork using HYDROPRO (*40*). The harmonic mean correlation time of 23 ns is quite close to the experimental value. Judging by the relative values of the preexponential factors β_i, about 75% of the motion in free 2AP Fork is rapid internal motion. Figure 5b shows an experiment for RNAP−2AP Fork complex with about 1×10^3 peak counts. Similar results were obtained from experiments with about 5×10^3 peak counts. The 1.4 ns correlation time indicates much slower internal motion of the base than in free 2AP Fork. Moreover, the bound RNAP appears to have reduced the amount of internal motion to half that in the free DNA. About 63% of the 2AP is completely immobilized by the enzyme. The long 110 ns correlation time is poorly resolved on the time scale of the anisotropy experiment, which is limited by the intensity-weighted lifetime $\langle\tau\rangle = \Sigma\alpha_i\tau_i^2/\Sigma\alpha_i\tau_i$ of the fluorophore. For 2AP in forked DNA, $\langle\tau\rangle$ values are 4.7 and 6.0 ns for free and bound 2AP Fork. Rotational correlations times 5-fold greater than $\langle\tau\rangle$ are not well-determined, so the 110 ns value should be considered a lower limit. This time scale limitation is also responsible for the similarity of the anisotropy decay curves in Figure 5a,b.

DISCUSSION

The use of forked DNAs (see Figure 1) as model templates for the study of RNAP−promoter interactions is predicated upon the specificity of the interaction. Previously, we and others had demonstrated the sensitivity of the interaction to base substitutions that also affect promoter utilization (*17*, *18*, *20*). The results of the footprinting and chemical probing experiments presented here indicate that the forked templates studied (Figure 1) behave similarly not only to their double-stranded variants, but also to promoter DNA. Thus, at the level of resolution of these experiments, the interactions of RNAP with the nontemplate strand in the melted region of an open complex are not dependent upon the presence of the template strand. The complexes between RNAP and forked DNA templates behave similarly to those between RNAP and promoter DNA in other respects as well. We had shown before that base substitutions in forked and promoter DNA had similar effects upon RNAP binding and that complexes of RNAP and Short Fork (see Figure 1) undergo isomerizations such as those seen for RNAP−promoter complexes (*20*). In aggregate, these results support the use of forked DNAs as model templates to simplify the study of particular facets of the interaction of RNAP with promoter DNA.

For the Duplex DNA, the presence of a 2AP base at −11 reduces by similar amounts the formation of heparin-resistant complexes with RNAP and RNAP-induced strand opening as probed by $KMnO_4$ sensitivity. This contrasts a recent report from Adhya's laboratory (*41*), that substitution of −11 A for 2AP at the promoters of the gal operon prevents strand opening by RNAP, even though a heparin-resistant complex is still formed. Our observation from both binding (Figure 2) and footprinting experiments (Figures 3 and 4) that 2AP substitution does not prevent formation of a heparin-resistant complex is in agreement with the above study (*41*). As reported here, Heyduk and co-workers (*42*) also found that the presence of a 2AP at −11 in a model template decreased the apparent binding affinity for RNAP. However, our observation that 2AP at position −11 in double-stranded DNA reduced, but did not prevent, RNAP-induced strand separation in the Duplex (Figure 4b) contradicts the previous finding that promoters bearing a 2AP at −11 did not undergo RNAP-induced strand separation (*41*). The observed discrepancy may result from our use of the Duplex template shown in Figure 1, rather than an intact promoter. Alternatively, the effects of 2AP substitution at −11 may be promoter-specific.

The environmentally sensitive intrinsic fluorescent probe, 2AP, is widely used to study DNA structure, dynamics, and interactions. Recently, increases in 2AP fluorescence intensity have been attributed to base flipping in enzyme-DNA complexes (*43*−*45*). RNAP holoenzyme has 19 tryptophans. Förster energy transfer from one or more tryptophans to 2AP would increase the intensity and depolarize the fluorescence of the bound 2AP Fork. Excitation of tryptophan and thereby distortions of quantum yield, lifetime, and anisotropy decay data due to energy transfer were avoided by exciting at 320 nm. Although considerably reducing fluorescence signals, this resulted in selective excitation of 2AP fluorescence in the RNAP complex. To our knowledge, this paper is the first report of time-resolved fluorescence anisotropy for a protein complex with 2AP-containing oligonucleotide.

While no X-ray or NMR structures of A- or B-form duplexes containing 2AP have been reported, 2AP was shown to form a Watson−Crick base pair with T that is only slightly weaker than an A−T base pair (*21*, *39*, *46*, *47*). Thus, the base analogue is not expected to greatly perturb double-stranded DNA structure. On the other hand, any process critically dependent on the 6-amino group of A at a particular position would be affected by 2AP substitution. Recently, Rachofsky et al. proposed a simple method for distinguishing three conformational states of 2AP in duplex DNA: intrahelical stacked, intrahelical unstacked, and extrahelical (*32*). We applied their analysis to the quantum yield and lifetime data of 2AP Fork. In the absence of RNAP, about 60% of the 2AP is stacked, with the remainder being partially unstacked. In the presence of RNAP, the apparent stacking increases to 80%. However, the method of Rachofsky et al. does not account for static and dynamic quenching of 2AP fluorescence by the protein. Stern−Volmer experiments show that aromatic amino acids quench the fluorescence of 2AP riboside (data not shown). Further investigation of the effects of protein functional groups on 2AP fluorescence are needed before 2AP base stacking can be determined in protein-nucleic acid complexes.

The most salient result of these studies is the large effect of RNAP on the rotational correlation times of the 2AP at −11. Two possible interpretations of the anisotropy data for the complex are: (1) The two anisotropy decay components of RNAP−2AP Fork represent two species of RNAP complex, tightly and weakly bound or open and closed. In this scenario, the 110 ns correlation time would correspond to tightly bound complex and the 1.4 ns correlation time to weakly bound complex. On the basis of the relative preexponential factors β_i, 63% of RNAP−2AP Fork complexes are tightly bound. This is in good agreement with the population of heparin-resistant RNAP−2AP Fork complex determined in the EMSA binding studies. (2) The two anisotropy decay components of RNAP−2AP Fork represent the range of mobility of the fluorescent base in the complex. As in the case of free 2AP Fork, all bound 2AP Fork exhibits both internal and overall tumbling motions. However, the internal motion of 2AP is substantially reduced in the complex. We conclude that RNAP is able to accommodate the 2AP, and by inference also an A at the equivalent position, in a tight pocket near the surface of the enzyme. This result is consistent with nucleation of DNA melting by flipping of the −11 A out of the duplex. While recently the structure of a complex between *Thermus aquaticus* RNA polymerase and a forked DNA was determined (*19*), providing much useful information concerning the alignment of the RNAP and the DNA, the 6.5 Å resolution is insufficient to pinpoint residues involved in formation of a binding pocket for the −11 A. Mutational studies from Gralla's and our groups (*12*, *15*, *16*, *26*) would suggest that such a pocket could include several aromatic amino acids from region 2.3 of σ^{70}, with likely candidates being Y430, W433, and W434. Confirmation of this assignment will have to await the determination of the effects of alanine substitutions for these aromatic residues on the correlation times of the 2AP at −11.

ACKNOWLEDGMENT

We thank Dr. Sankar Adhya for his comments on a draft of the manuscript, Dr. Lawrence C. Sowers for a gift of 2AP riboside, and Dr. M. Caprara for help with the DEPC reactions.

REFERENCES

1. Zhang, G., Campbell, E. A., Minakhin, L., Richter, C., Severinov, K., and Darst, S. A. (1999) *Cell 98*, 811−824.
2. Siebenlist, U., Simpson, R. B., and Gilbert, W. (1980) *Cell 20*, 269−281.
3. Record Jr., M. T., Reznikoff, W. S., Craig, M. L., McQuade, K. L., and Schlax, P. J. (1996) in *Escherichia coli and Salmonella, Cellular and Molecular Biology* (Neidhardt, F. C., Ed.) pp 792−820, ASM Press, Washington, DC.
4. Zaychikov, E., Denissova, L., Meier, T., Gotte, M., and Heumann, H. (1997) *J. Biol. Chem. 272*, 2259−2267.
5. deHaseth, P. L., Zupancic, M., and Record Jr., M. T. (1998) *J. Bacteriol. 180*, 3019−3025.
6. Mekler, V., Kortkhonjia, E., Mukhopadhyay, J., Knight, J., Revyakin, A., Kapanidis, A. N., Niu, W., Ebright, Y. W., Levy, R., and Ebright, R. H. (2002) *Cell 108*, 599−614.
7. Roe, J. H., Burgess, R. R., and Record, M. T. (1984) *J. Mol. Biol. 176*, 495−521.
8. Roe, J. H., Burgess, R. R., and Record Jr., M. T. (1985) *J. Mol. Biol. 184*, 441−453.
9. Buc, H., and McClure, W. R. (1985) *Biochemistry 24*, 2712−2723.
10. Saecker, R. M., Tsodikov, O. V., McQuade, K. L., Schlax, P. E., Capp, M. W., and Record, M. T., Jr. (2002) *J. Mol. Biol. 319*, 649−671.
11. Craig, M. L., Tsodikov, O. V., McQuade, K. L., P. E. Schlax, J., Capp, M. W., Saecker, R. M., and Record Jr., M. T. (1998) *J. Mol. Biol. 283*, 741−756.
12. Juang, Y.-L., and Helmann, J. D. (1994) *J. Mol. Biol. 235*, 1470−1488.
13. Juang, Y.-L., and Helmann, J. D. (1995) *Biochemistry 34*, 8465−8473.
14. Helmann, J. D., and deHaseth, P. L. (1999) *Biochemistry 37*, 5959−5967.
15. Fenton, M. S., Lee, S. J., and Gralla, J. D. (2000) *EMBO J. 19*, 1130−1137.
16. Tomsic, M., Tsujikawa, L., Panaghie, G., Wang, Y., Azok, J., and deHaseth, P. L. (2001) *J. Biol. Chem. 276*, 31891−31896.
17. Guo, Y., and Gralla, J. D. (1998) *Proc. Natl. Acad. Sci. U.S.A. 95*, 11655−11660.
18. Fenton, M. S., and Gralla, J. D. (2001) *Proc. Natl. Acad. Sci. U.S.A. 98*, 9020−9025.
19. Murakami, K. S., Masuda, S., Campbell, E. A., Muzzin, O., and Darst, S. A. (2002) *Science 296*, 1285−1290.
20. Tsujikawa, L., Tsodikov, O. V., and deHaseth, P. L. (2002) *Proc. Natl. Acad. Sci. U.S.A. 99*, 3493−3498.
21. Sowers, L. C., Fazakerley, G. V., Eritja, R., Kaplan, B. E., and Goodman, M. F. (1986) *Proc. Natl. Acad. Sci. U.S.A. 83*, 5434−5438.
22. Burgess, R. R., and Jendrisak, J. J. (1975) *Biochemistry 14*, 4634−4638.
23. Gonzales, N., Wiggs, J., and Chamberlin, M. J. (1977) *Arch. Biochem. Biophys. 182*, 404−408.
24. Galas, D. J., and Schmitz, A. (1978) *Nucleic Acids Res 5*, 3157−3170.
25. Sasse-Dwight, S., and Gralla, J. D. (1989) *J. Biol. Chem. 264*, 8074−8081.
26. Panaghie, G., Aiyar, S. E., Bobb, K. L., Hayward, R. S., and deHaseth, P. L. (2000) *J. Mol. Biol. 299*, 1217−1230.
27. Liu, B., Barkley, M. D., Morales, G. A., McLaughlin, M. L., and Callis, P. R. (2000) *J. Phys. Chem. B 104*, 1837−1843.
28. Melhuish, W. H. (1961) *J. Phys. Chem. 65*, 229−235.
29. Liu, W., Chen, Y., Watrob, H., Bartlett, S. G., Jen-Jacobson, L., and Barkley, M. D. (1998) *Biochemistry 37*, 15457−15465.
30. Beechem, J. M. (1989) *Chem. Phys. Lipids 50*, 237−251.
31. Rachofsky, E. L., Osman, R., and Ross, J. B. A. (2001) *Biochemistry 40*, 946−956.
32. Rachofsky, E. L., Seibert, E., Stivers, J. T., Osman, R., and Ross, J. B. A. (2001) *Biochemistry 40*, 957−967.
33. Guest, C. R., Hochstrasser, R. A., Sowers, L. C., and Millar, D. P. (1991) *Biochemistry 30*, 3271−3279.
34. Ozoline, O. N., and Tsyganov, M. A. (1995) *Nucleic Acids Res. 23*, 4533−4541.
35. Beechem, J. M., Otto, M. R., Bloom, L. B., Eritja, R., Reha-Krantz, L. J., and Goodman, M. F. (1998) *Biochemistry 37*, 10144−10155.
36. Smagowicz, J., and Wierzchowski, K. L. (1974) *J. Lumin. 8*, 210−232.
37. Holmén, A., Nordén, B., and Albinsson, B. (1997) *J. Am. Chem. Soc. 119*, 3114−3121.
38. Ward, D. C., Reich, E., and Stryer, L. (1969) *J. Biol. Chem. 244*, 1228−1237.
39. Nordlund, T. M., Anderson, S., Nilsson, L., Rigler, R., Graslund, A., and McLaughlin, L. W. (1989) *Biochemistry 28*, 9095−9103.
40. Fernandes, M. X., Ortega, A., López, M. C., and García de la Torre, J. (2002) *Nucleic Acids Res. 30*, 1782−1788.
41. Lim, H. M., Lee, H. J., Roy, S., and Adhya, S. (2001) *Proc. Natl. Acad. Sci. U.S.A. 98*, 14849−14852.
42. Matlock, D. L., and Heyduk, T. (2000) *Biochemistry 39*, 12274−12283.
43. Allan, B. W., and Reich, N. O. (1996) *Biochemistry 35*, 14757−14762.
44. Stivers, J. T. (1999) *Biochemistry 38*, 952−963.
45. Christine, K. S., MacFarlane IV, A. W., Yang, K., and Stanley, R. J. (2002) *J. Biol. Chem. 277*, 38339−38344.
46. Wu, P., and Nordlund, T. M. (1990) *Biochemistry 29*, 6508−6514.
47. Law, S. M., Eritja, R., Goodman, M. F., and Breslauer, K. J. (1996) *Biochemistry 35*, 12329−12337.

BI026539M